


Inversionless Gain in a Lossy Medium

Eliran Talker,^{*} Yefim Barash, Noa Mazurski, and Uriel Levy[†]

Department of Applied Physics, The Faculty of Science, The Center for Nanoscience and Nanotechnology, The Hebrew University of Jerusalem, Jerusalem 91904, Israel

 (Received 20 November 2022; revised 2 April 2023; accepted 12 May 2023; published 6 July 2023)

We study gain without inversion due to coherence effects in a Doppler-broadened degenerate three-level system of a rubidium-hydrogen mixture in a miniaturized micron-scale custom vapor cell. The cell miniaturization gives rise to collisions of atoms with the walls of the cell. This, combined with the high collision rate with the hydrogen buffer gas, allows us to observe gain in the absorption spectra. Furthermore, we analyze the role of cell miniaturization in the evolution of the gain profile. In addition to fundamental interest, the observation of gain without inversion in our miniaturized cells paves the way for applications such as miniaturized lasers without inversion.

DOI: [10.1103/PhysRevApplied.20.014007](https://doi.org/10.1103/PhysRevApplied.20.014007)

I. INTRODUCTION

Atomic coherence effects, such as a coherent population trapping [1–7], electromagnetically induced transparency [5,8–15], high index of refraction with vanishing absorption, and amplification and lasing without inversion (AWI and LWI) have been intensively investigated over recent years due to their fundamental properties and their multiple potential applications [16–24], ranging from laser cooling to isotope separation and from ultrahigh-sensitivity magnetometers to the generation of giant pulses of laser light. Among these phenomena, AWI and LWI have received considerable attention for their potential to obtain laser light in diverse spectral domains, e.g., the x-ray range where conventional methods based on population inversion are not available or are difficult to implement.

In the present work, we demonstrate, for the first time, gain without population inversion in a micron-scale Rubidium vapor cell without the use of an incoherent pump beam. The demonstrated effects take advantage of the frequent atom-wall collisions in our micrometer cell as well as the frequent collisions with the buffer gas (hydrogen) to suppress the optical pumping. In the following, we describe the theoretical background and the simulations of gain and populations in different types of cells. This is followed by a description the experimental setup and the obtained experimental results.

II. THEORY AND SIMULATIONS

To analyze the rubidium (Rb) hot vapor system, in the presence of buffer gas and wall collisions, we consider a model as shown in Fig. 1, which consists of four levels labeled $|1\rangle$, $|2\rangle$, $|3\rangle$, and $|4\rangle$. We assume a

high-power pump beam, which allows us to excite all the energy levels of the D_2 hyperfine manifold at the same time due to power broadening, and thus the excited states can be treated as a single state instead of separate states. Regarding the probe beam in the D_1 transition line, there is a large separation between the two hyperfine excited states, of about 361 MHz. Owing to this large separation, we can consider only one of the hyperfine excited states. To ensure accurate experimental results, we need to cancel out the Zeeman levels of the excited and ground states. We accomplish this by setting the external magnetic field to zero, which is achieved experimentally using four layers of mu-metal. A strong driving field induces a coherent coupling between levels $|1\rangle$ and $|4\rangle$, whereas a weak probe beam is scanned around the transition between levels $|1\rangle$ and $|3\rangle$. Under the rotating wave approximation, the Hamiltonian of the system, including the interaction between the atoms and the two electromagnetic fields can be written as

$$\begin{aligned} H &= H_1 + H_2 \\ H_1 &= \hbar\omega_{\text{pr}}a_3^\dagger a_3 + \hbar\omega_{\text{pu}}a_4^\dagger a_4 \\ H_2 &= \hbar\Delta_{\text{pr}}a_3^\dagger a_3 + \hbar\Delta_{\text{pu}}a_4^\dagger a_4 + \hbar[\Omega_{\text{pr}}a_3^\dagger a_1 \\ &\quad + \Omega_{\text{pu}}a_4^\dagger a_1 + \text{c.c.}] \end{aligned} \quad (1)$$

where \hbar is Planck constant, a , a^\dagger are the lowering and raising operator respectively. $\Delta_{\text{pr}} = \omega_{\text{pr}} - \omega_{13}$ and $\Delta_{\text{pu}} = \omega_{\text{pu}} - \omega_{14}$ are the detunings, and ω_{13} and ω_{14} denote the frequencies of the transitions from $|1\rangle$ to $|3\rangle$ and $|1\rangle$ to $|4\rangle$, respectively. ω_{pr} and ω_{pu} are the probe and the pump beam frequencies respectively. Ω_{pr} and Ω_{pu} are the Rabi frequencies of the probe and the pump fields. The time evolution of the density operators is described by the Liouville equation,

$$\partial_t \rho = -\frac{i}{\hbar}[H, \rho] - \frac{1}{2}\{\Gamma, \rho\} + \Lambda, \quad (2)$$

^{*}eliran.talker@mail.huji.ac.il

[†]ulevy@mail.huji.ac.il

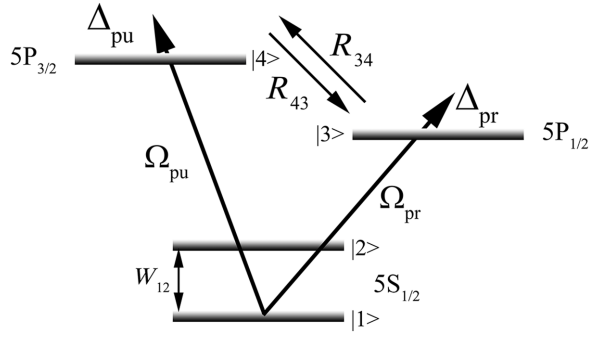


FIG. 1. Schematic diagram level of rubidium vapor. W_{12} is the population exchange rate of the ground levels Ω_{pr} , Ω_{pu} are the Rabi frequencies of the probe and the pump beam, respectively; R_{34}, R_{43} are the energy transfers rates between excited states due to buffer gas collisions; Δ_{pr}, Δ_{pu} are the probe and pump detunings.

where the square brackets denote the commutator, and the curly brackets stand for the anticommutator. We assume that the upper states $|3\rangle$ and $|4\rangle$ decay spontaneously with rates γ_3 and γ_4 , respectively [25,26]. In addition to spontaneous relaxation, we must also take into account the influence of buffer gas. Buffer gas can lead to the transfer of population from excited states through collisional processes (denoted as R_{34} and R_{43}). Furthermore, pressure broadening relaxation should be considered as well. The overall relaxation is described by the matrix Γ ,

$$\Gamma = W_{12}|1\rangle\langle 1| + W_{12}|2\rangle\langle 2| + (\gamma_3 + R_{34} + \gamma_{\text{wall}})|3\rangle\langle 3| + (\gamma_4 + R_{43} + \gamma_{\text{wall}})|4\rangle\langle 4|. \quad (3)$$

W_{12} is the wall collision relaxation (see Supplemental Material [31]). R_{34}, R_{43} are the collisional transfer rates between $5P_{1/2}$ and $5P_{3/2}$ levels due to the buffer gas (for more information see Supplemental Material [31]). We use here the simple model of ground state relaxation. Λ is related to the repopulated matrix (see Supplemental Material [31]). The evolution equation for the atomic coherence related to the absorption as obtained from Eq. (2) is equal to (see Supplemental Material [31])

$$\rho_{13} = \frac{2\Omega_{pr}i(\rho_{33} - \rho_{11}) + 2i\Omega_{pu}\rho_{43}}{R + W_{12} + \gamma_3 + 2i\Delta_{pr}}. \quad (4)$$

From the numerator of Eq. (4) we see that there are two contributions of the coherence (ρ_{13}) that modify the usual gain and absorption. The first is the dynamical Stark effect [27], studied theoretically and experimentally in a V-type configuration in Ref. [28]. There is, however, another effect that modifies the properties of the V scheme. This contribution is represented by the coherence effect of the two excited states (ρ_{43}).

Figure 2(a) shows the evolution of the population of the ground states and the excited states as a function of time. The relaxation rate (W_{12}) between the ground states due to wall collisions is assumed to be $W_{12} \sim 0.5\gamma_3$, corresponding to approximately 8 Torr of H_2 buffer gas. The wall collision suppresses the optical pumping. Therefore, the population difference $\rho_{33} - \rho_{11}$ is determined by the rates at which atoms leave and decay into states $|1\rangle$ and $|2\rangle$. In the limit of a weak probe beam, atoms can leave state $|1\rangle$ only by being pumped to state $|4\rangle$. It is worth mentioning that if level $|2\rangle$ decays faster than level $|4\rangle$, an inversion of the transition coupled by the weak probe field cannot be achieved [see Fig. 2(b)]. By observing the steady-state values, we see that the value of ρ_{13} is positive [Figs. 2(b) and 2(c)], hence gain is achieved in spite of the fact that $\rho_{33} - \rho_{11}$ is negative, giving rise to gain without inversion.

We now address the case of a large cell with negligible wall collisions by repeating the calculations, this time with $W_{12} = 0$. Figure 3(a) shows that when wall collisions are negligible the population of the ground state $|2\rangle$ is increased due to optical pumping. As a result, the coherence of the levels $|3\rangle$ and $|4\rangle$ is diminished [i.e., ρ_{43} is nulled, see Fig. 3(c)], and ρ_{13} becomes negative. As such, observing gain without inversion becomes impossible in this case.

Next, we calculate the gain (absorption) coefficient as a function of probe detuning for a weak probe field on the $|1\rangle$ to $|3\rangle$ transition. As mentioned previously, the gain is proportional to the imaginary part of the off-diagonal elements of the atomic density matrix ρ_{13} . In the weak probe field, and under the condition of the pump being at resonance, we obtain the following expression for the frequency-dependent susceptibility:

$$\begin{aligned} \chi^{(5S_{1/2} \rightarrow 5P_{1/2})}(\Delta_{pr}, \nu) &= \frac{3\lambda_{pr}^2 NL \gamma_3}{4\pi} \frac{\text{Im}(\rho_{13}(\Delta_{pr}, \nu))}{\Omega_{pr}} \\ &= \frac{3\lambda_{pr}^2 NL \gamma_3}{4\pi \Omega_{pr}} \frac{2(R + W_{12} + \gamma_3)}{(R + W_{12} + \gamma_3)^2 + (2\Delta_{pr})^2} \\ &\quad (\Omega_{pu}\rho_{43}(\Delta_{pr}, \nu) + \Omega_{pr} \\ &\quad (\rho_{33}(\Delta_{pr}, \nu) - \rho_{11}(\Delta_{pr}, \nu))). \end{aligned} \quad (5)$$

Where N is the atomic density and L is the cell length. From Eq. (5) (see right parenthesis of the second equality) we can identify two contributions that affect the gain-absorption terms. The first is related to the coherence of the two excited states, ρ_{43} , while the second corresponds to the population inversion of the ground state and the excited state of the probe beam, $\rho_{33} - \rho_{11}$. Therefore, as mentioned previously, we can observe gain in the

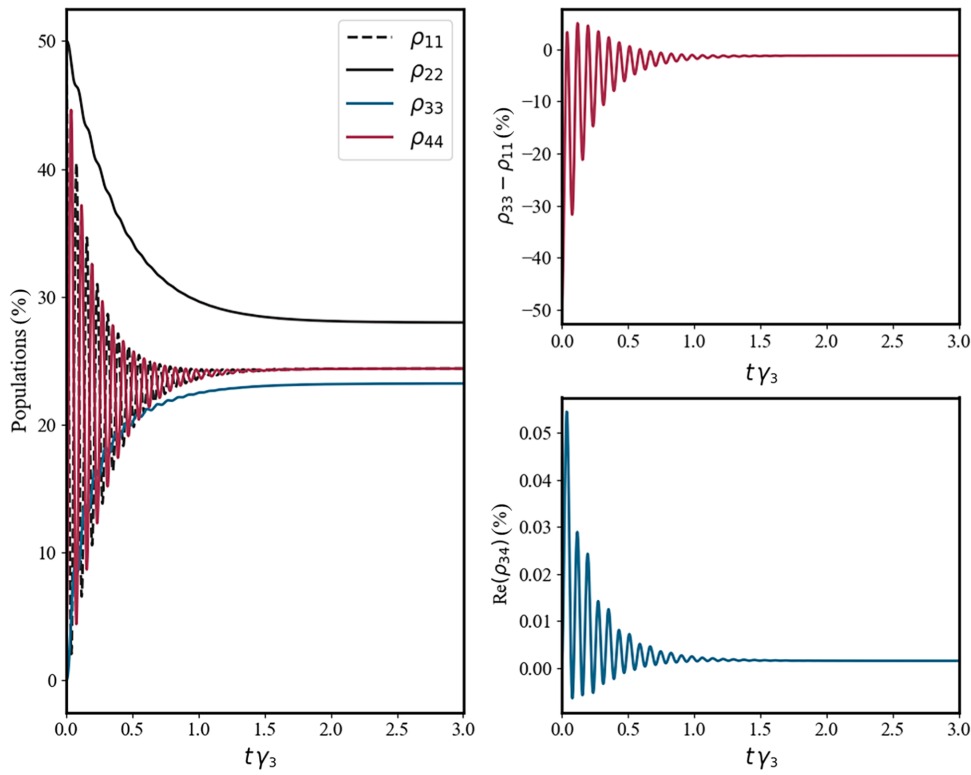


FIG. 2. Time evolution of the density matrix as calculated from the four-level optical Bloch model, with parameters of $\Omega_{\text{pr}} = 0.1\gamma_3$, $\Omega_{\text{pu}} = 90\gamma_3$, $W_{12} = 6\gamma_3$, $R_{34} = R_{43} = 10\gamma_3$, $\gamma_3 = 2\pi 5.75$ MHz, and $\gamma_4 = 2\pi 6.06$ MHz.

absorption although there is no population inversion (i.e., $\rho_{33} - \rho_{11} < 0$). In order to calculate the actual gain while taking into account the Doppler effect, which is a dominant factor in our hot vapor system, we multiply the susceptibility by the Boltzmann distribution and integrate over all

velocities.

$$G(\Delta_{\text{pr}}) = \int_{-\infty}^{\infty} \chi(\Delta_{\text{pr}}, v) \exp\left(-\frac{v^2}{u^2}\right) dv \quad (6)$$

where u is the most probable velocity.

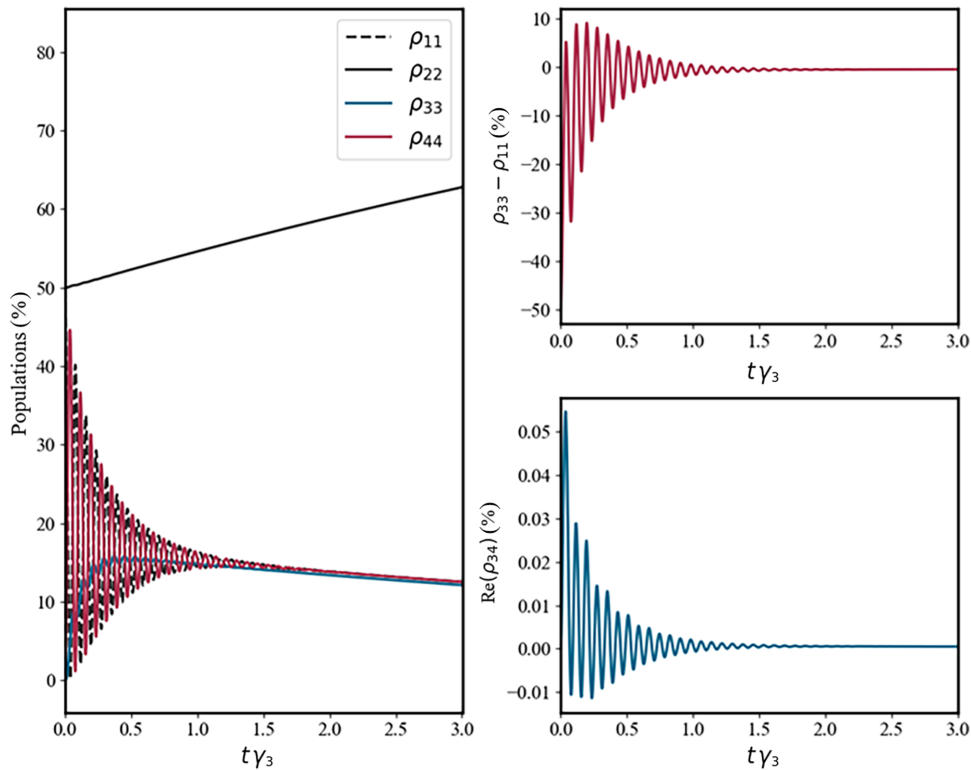


FIG. 3. Time evolution of the density matrix as calculated from the four-level optical Bloch model, with parameters of $\Omega_{\text{pr}} = 0.1\gamma_3$, $\Omega_{\text{pu}} = 90\gamma_3$, $W_{12} = 0$, $R_{34} = R_{43} = 10\gamma_3$, $\gamma_3 = 2\pi 5.75$ MHz, and $\gamma_4 = 2\pi 6.06$ MHz.

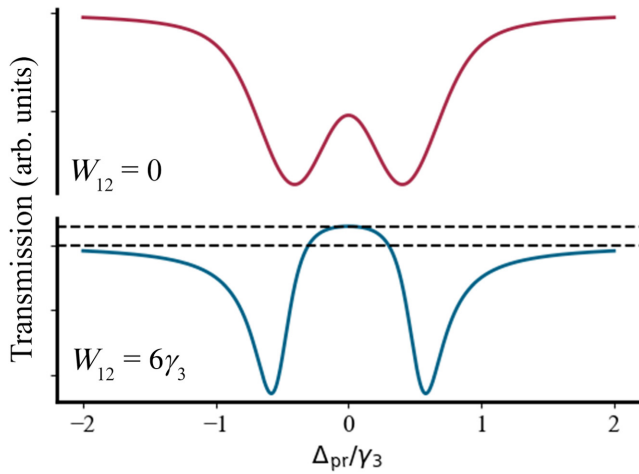


FIG. 4. Simulation of the transmission spectra as a function of the probe detuning with and without ground state relaxation (W_{12}) due to wall collisions. In both plots the parameter are $\Delta_{\text{pu}} = 0$, $\Omega_{\text{pr}} = 0.05\gamma_3$, $\Omega_{\text{pu}} = 60\gamma_3$, $R_{34} = R_{43} = 2\gamma_3$, $\gamma_3 = 2\pi 5.75$ MHz, and $\gamma_4 = 2\pi 6.06$ MHz.

Figure 4 shows transmission spectra for the two different cases of negligible collisions ($W_{12} = 0$, red line), and significant collisions ($W_{12} = 6\gamma_3$, blue line). Indeed, when the collision effect is negligible, we cannot observe gain in the transmission, whereas when the wall collision rate is significant one can observe gain within the transmission spectra.

Next, we turn to study the influence of the relaxation mechanisms (e.g., wall collision) on the gain obtained in the absorption spectrum. As shown in Eq. (5) the susceptibility at the resonance transition is dependent upon the imaginary part of the coherence element ρ_{13} and can be written as (see Supplemental Material [31])

$$\chi^{(SS_{1/2} \rightarrow 5P_{1/2})} = G[(\rho_{33} - \rho_{11}) + \Omega_{\text{pu}}^{*2}(\rho_{11} - \rho_{44})], \quad (7)$$

where

$$\Omega_{\text{pu}}^{*2} = \frac{\Omega_{\text{pu}}^2}{\gamma_{\text{eff}}}, \quad (8)$$

$$G = \frac{3\lambda_{\text{pr}}^2 N L \gamma_3}{2\pi(R + W_{12} + \gamma + \gamma_{\text{wall}} + \Omega_{\text{pu}}^2(\gamma_{\text{tot}}/\gamma_{\text{eff}}))}. \quad (9)$$

The susceptibility is dependent upon two factors. The first is known as the dynamical Stark effect. The second contribution is represented by the term proportional to the Ω_{pu}^{*2} in the second term of Eq. (7) and is precisely due to the quantum interference of the absorption. It follows from Eq. (7) that absorption interferes destructively if $\rho_{11} - \rho_{44} > 0$. This leads to a reduction of absorption and enhancement of the gain. As a result, the probe field can be amplified even if $\rho_{33} - \rho_{11} < 0$. The effective pump is dependent upon the

Experimental setup and results

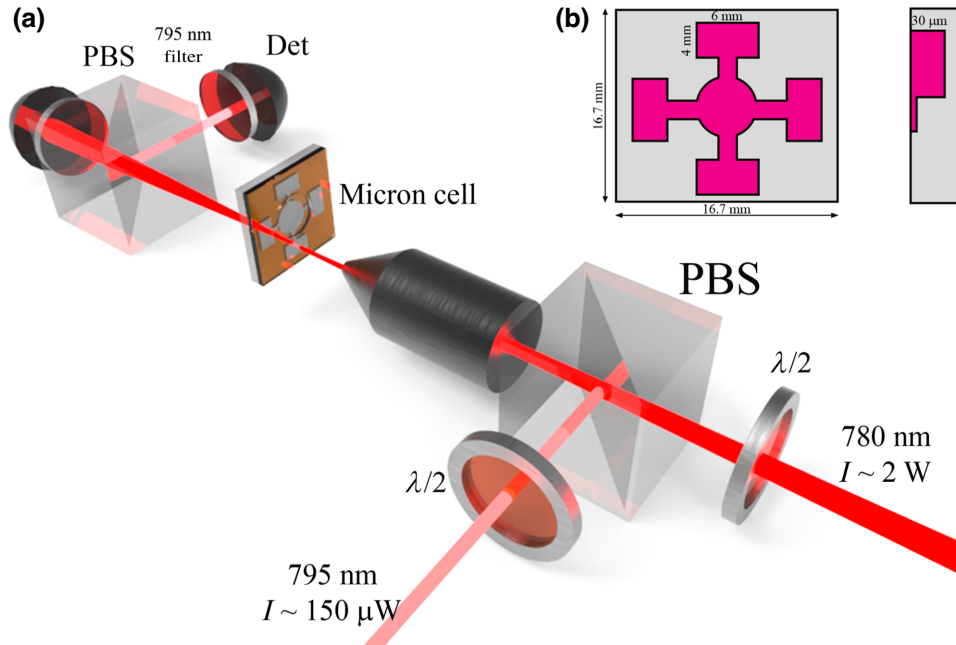


FIG. 5. (a) Illustration of the experimental setup used for the entire results. PBS, polarizing beam splitter; Det, detector. (b) Top view of the device and side cross-section schematic (not to scale) of the micrometer rubidium cell.

relaxation mechanisms by

$$\Omega_{\text{pu}}^{*2} = \frac{\Omega_{\text{pu}}^2}{\gamma_{\text{eff}}}. \quad (10)$$

So, to obtain gain we need to set the pump beam to satisfy

$$\Omega_{\text{pu}}^2 > \frac{1}{2}(R^2 + \gamma_{\text{wall}}^2 + 2R\gamma_{\text{wall}}). \quad (11)$$

By choosing this parameter we can obtain gain in the absorption signal. It is worth mentioning that, as shown by Eq. (9), the relaxation effects reduce the overall contrast. The reduced contrast should be taken into account when performing experiments in this system.

III. EXPERIMENTAL SETUP AND RESULTS

An illustration of our experimental setup consisting of two laser beams is shown in Fig. 5(a). The pump beam wavelength is 780 nm, corresponding to the D_2 transition ($5S_{1/2}-5P_{3/2}$) of the Rb vapor. This laser has a short-term linewidth on the order of 100 kHz, and its frequency is stabilized to the $F_g = 2 \rightarrow F_e = 3$ transition using the well-known saturated absorption spectroscopy technique [29]. As shown in the previous section, to obtain gain we need to generate a strong excited state coherence. This is done by setting the pump intensity to be fairly high, around 2 W, by using a tapered amplifier (Toptica BOOSTA). The probe beam is tuned to the wavelength of 795 nm, corresponding to the D_1 transition ($5S_{1/2}-5P_{1/2}$) of Rb. It is kept at a relatively low intensity level of around $150 \mu\text{W}$. At such intensity levels, we do not change the population distribution of the system, but only measure the probe transmission through the miniaturized cell, in the presence of wall collisions and buffer gas, and under the condition of strong pump beam intensity. The linewidth of the probe beam laser is around 100 kHz.

As mentioned previously, in order to observe gain we need the wall collision rate to be significant with respect to the excited state decay rate. To facilitate such a case, we fabricate a custom miniaturized vapor cell with thickness of about $30 \mu\text{m}$ along the light propagation direction. A schematic description of the cell geometry is given in Fig. 5(b). For more details related to the cell fabrication method see Ref. [30].

To eliminate the Zeeman sublevel splitting, the residual magnetic field is canceled using a fourfold mu-metal shield, which reduces the residual magnetic field to less than 10^{-7} T. The magnetic shielding is used to reduce the optical pumping effect because of the equal probabilities of occupying each Zeeman sublevel. The experiments are done at elevated temperatures in the range of 150–250 °C corresponding to atomic densities of $3.5 \times 10^{19} \text{ m}^{-3}$ and $3.05 \times 10^{20} \text{ m}^{-3}$, respectively. These high temperatures

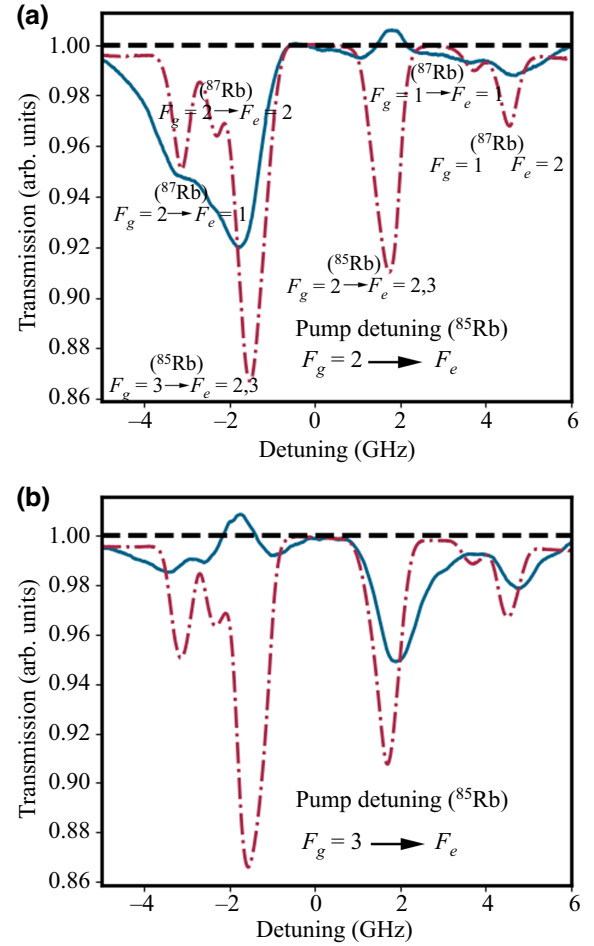


FIG. 6. D_1 line transmission for natural rubidium in micrometer vapor cell at temperature of 150 °C where the pump beam is fixed at the $F_g = 3 \rightarrow F_e$ transition (a) and $F_g = 2 \rightarrow F_e$ transition (b) of ^{85}Rb . The pump beam (780 nm) intensity is about 2 W and the probe intensity is around $150 \mu\text{W}$ (795 nm). Red dotted line represents the transmission of a reference cell at room temperature.

allow us to reach high optical densities even at low propagation length. Furthermore, by increasing the temperature we increase the most probable velocity and as a result the wall collision rate is increased, further enhancing the effect of gain without inversion.

In order to detect only the probe beam while eliminating the detection of the pump beam, we set the pump beam to be TE polarized while the probe beam is set to be TM polarized. By using a polarizing beam splitter after the vapor cell we filter out the TE mode and detect only the TM mode. To further improve the filtering, we add a bandpass filter around 795 nm allowing only the probe to be transmitted, while rejecting the pump at 780 nm.

Using the previously described setup, we measure the transmission spectrum of light through the miniaturized vapor cell, as shown in Fig. 6. The red dotted lines in Fig. 6

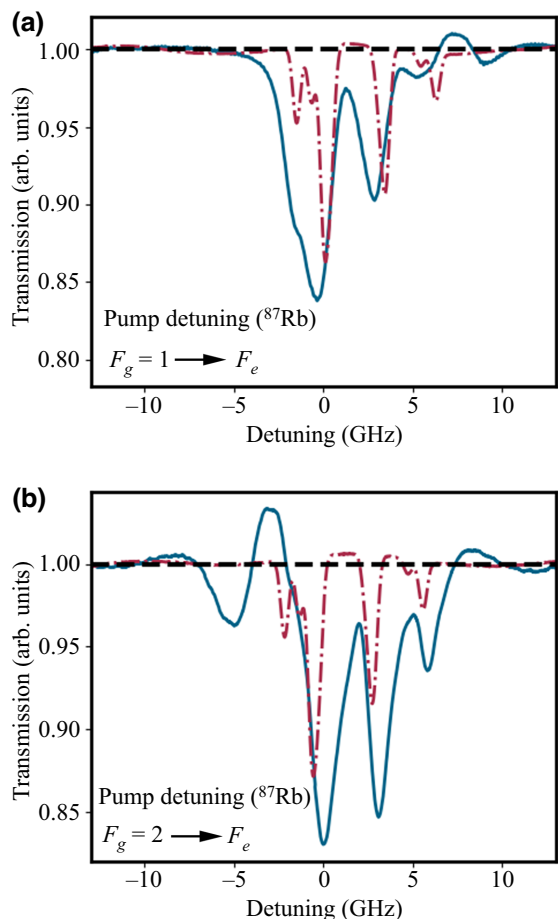


FIG. 7. D_1 line transmission for natural rubidium in micrometer vapor cell at temperature of 250 °C where the pump beam is fixed at the $F_g = 1 \rightarrow F_e$ transition (a) and $F_g = 2 \rightarrow F_e$ transition (b) of ^{87}Rb . The pump beam (780 nm) intensity is about 2 W and the probe intensity is around 150 μW (795 nm). Red dotted line represents the transmission of a reference cell at room temperature.

represent the transmission spectra of the D_1 transition of natural Rb vapor measured in a 7.5-cm-long reference cell at room temperature (25 °C), while the blue lines represent the transmission spectra obtained from our 30- μm -thick cell at a temperature of 150 °C. In the top panel [Fig. 6(a)] the pump is parked at the $F_g = 2 \rightarrow F_e$ transition of ^{85}Rb , whereas in the bottom panel [Fig. 6(b)], the pump is parked on the $F_g = 3 \rightarrow F_e$ transition of ^{85}Rb . Because the use of the thin cell results in a low optical density, the overall contrast is approximately 5% even at these elevated temperatures. The line width of the transmission spectra obtained from the 30- μm cell is broader than the transmission measured from the reference cell, mainly because of power broadening, increased Doppler broadening (due to the elevated temperatures), and pressure broadening (due to the presence of the buffer gas).

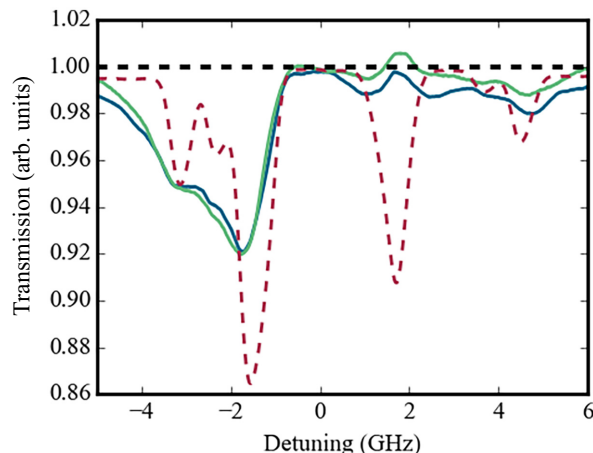


FIG. 8. D_1 line transmission of natural rubidium micrometer vapor cell without modulation (green line) and with modulation (blue line). The parameters are temperature of 200 °C, pump beam (780 nm) intensity of about 2 W, and probe intensity of around 150 μW (795 nm). The pump is aligned to the $F_g = 2 \rightarrow F_e$ transition of ^{85}Rb . Red dotted line represents the transmission of the probe through a reference cell at room temperature.

In both cases [Figs. 6(a) and 6(b)], we observe gain in the transmission spectra. The observed gain from our 30- μm -long cell is approximately 1%, validating our assumption of inversionless gain. As predicted, the spectral lines in our cells are broader than the spectral lines in the reference cell. This is attributed to the combined effect of pressure broadening, power broadening, and enhanced Doppler broadening.

In Fig. 7 we repeat the same experiments; however, this time the pump beam is set to the ^{87}Rb resonance transitions. To reach significant contrast in the ^{87}Rb (approximately only 27% in natural rubidium), we need to increase the optical density. To do so, the temperature is increased to 250 °C. Indeed, when the pump is aligned to the $F_g = 1 \rightarrow F_e$ transition [Fig. 7(a)] the observed absorption contrast is around 12% and the gain is around 2%. Furthermore, for the stronger transition $F_g = 2 \rightarrow F_e$ [Fig. 7(b)] the observed gain approaches 4%.

One of the primary reasons for the increased gain observed in Fig. 6 as compared to Fig. 7 is the use of elevated temperature, which leads to enhanced collisional transfer rates (R_{34}, R_{43}), thereby resulting in an increase in gain. Furthermore, as illustrated in Fig. 7, the buffer gas spectrum shows a noticeable shift from the reference signal, owing to its strong dependence on temperature. Thus, as the temperature of the cell is significantly increased, the buffer gas shift is expected to increase as well. In order to verify that the gain results from coherence rather than from population inversion, we repeat the results of Fig. 6(a); however, this time we increase the laser linewidth by modulating the current of the diode laser with a noisy signal. By doing so, the linewidth is increased, allowing us to destroy

the coherence while maintaining the population distribution. In Fig. 8 we present the transmitted probe signal with (blue curve) and without (green curve) laser modulation. As can be seen, only the green curve shows gain, whereas the gain disappears for the blue curve.

IV. CONCLUSION

We demonstrate theoretically and experimentally the existence of gain without population inversion in miniaturized vapor cells of rubidium. The effect is a direct result of coherence between excited states. To achieve the condition of gain without population inversion we use buffer gas and a miniaturized vapor cell. The use of the buffer gas increases the population transition rate from level 4 to level 3, whereas the miniaturized cell results in the enhancement of the collision rate, destroying the optical pumping and allowing constant transition from the ground state to level 4 by the pump. Our results may pave the way to the demonstration of laser without inversion in miniaturized vapor cells.

ACKNOWLEDGMENTS

E.T acknowledges financial support from the Center for Nanoscience and Nanotechnology of the Hebrew University. The research was supported by a grant from the Israeli Science Foundation (ISF).

-
- [1] J. Vanier, Atomic clocks based on coherent population trapping: A review, *Appl. Phys. B Lasers Opt.* **81**, 421 (2005).
- [2] J. M. Danet, O. Kozlova, P. Yun, S. Guérande, and E. De Clercq, Compact atomic clock prototype based on coherent population trapping, *EPJ Web Conf.* **77**, 20 (2014).
- [3] S. Gozzini, L. Marmugi, A. Lucchesini, S. Gateva, S. Cartaleva, and K. Nasyrov, Narrow structure in the coherent population trapping resonance in sodium, *Phys. Rev. A* **84**, 013812 (2011).
- [4] A. Huss, R. Lammegger, L. Windholz, E. Alipieva, S. Gateva, L. Petrov, E. Taskova, and G. Todorov, Polarization-dependent sensitivity of level-crossing, coherent-population-trapping resonances to stray magnetic fields, *J. Opt. Soc. Am. B* **23**, 1729 (2006).
- [5] Y. Xiao, I. Novikova, D. F. Phillips, and R. L. Walsworth, Repeated interaction model for diffusion-induced Ramsey narrowing, *Opt. Express* **16**, 14128 (2008).
- [6] M. Abdel Hafiz and R. Boudot, A coherent population trapping Cs vapor cell atomic clock based on push-pull optical pumping, *J. Appl. Phys.* **118**, 2 (2015).
- [7] A. Mikata, U. Tanaka, and S. Urabe, Thin-cell sub-Doppler spectroscopy by spatially separated beam method and pump-probe method, *Appl. Opt.* **47**, 639 (2008).
- [8] E. Talker, P. Arora, Y. Barash, L. Stern, and U. Levy, Plasmonic enhanced EIT and velocity selective optical pumping measurements with atomic vapor, *ACS Photonics* **5**, 2609 (2018).
- [9] S. E. Harris, J. E. Field, and A. Imamoglu, Nonlinear Optical Processes Using Electromagnetically Induced Transparency, *Phys. Rev. Lett.* **64**, 1107 (1990).
- [10] R. P. Abel, A. K. Mohapatra, M. G. Bason, J. D. Pritchard, K. J. Weatherill, U. Raitzsch, and C. S. Adams, Laser frequency stabilization to excited state transitions using electromagnetically induced transparency in a cascade system, *Appl. Phys. Lett.* **94**, 071107 (2009).
- [11] D. F. Phillips, A. Fleischhauer, A. Mair, R. L. Walsworth, and M. D. Lukin, Storage of Light in Atomic Vapor, *Phys. Rev. Lett.* **86**, 783 (2001).
- [12] M. Shuker, O. Firstenberg, R. Pugatch, A. Ron, and N. Davidson, Storing Images in Warm Atomic Vapor, *Phys. Rev. Lett.* **100**, 223601 (2008).
- [13] M. D. Lukin and A. Imamoglu, Controlling photons using electromagnetically induced transparency, *Nature* **413**, 273 (2001).
- [14] Y. Li, S. Jin, and M. Xiao, Observation of an electromagnetically induced change of absorption in multilevel rubidium atoms, *Phys. Rev. A* **51**, R1754 (1995).
- [15] D. McGloin, Coherent effects in a driven vee scheme, *J. Phys. B: At., Mol. Opt. Phys.* **36**, 2861 (2003).
- [16] S. E. Harris, Lasers without Inversion: Interference of Lifetime-Broadened Resonances, *Phys. Rev. Lett.* **62**, 80 (1989).
- [17] H. Wu, M. Xiao, and J. Gea-Banacloche, Evidence of lasing without inversion in a hot rubidium vapor under electromagnetically-induced-transparency conditions, *Phys. Rev. A* **78**, 041802 (2008).
- [18] A. S. Zibrov, M. D. Lukin, D. E. Nikonov, L. Hollberg, M. O. Scully, V. L. Velichansky, and H. G. Robinson, Experimental Demonstration of Laser Oscillation without Population Inversion via Quantum Interference in Rb, *Phys. Rev. Lett.* **75**, 1499 (1995).
- [19] A. K. Popov, S. A. Myslivets, J. Y. Gao, H. Z. Zhang, and B. Welleghausen, Inversionless gain in a three-level system driven by a strong field and collisions, *Chin. Phys.* **9**, 124 (2000).
- [20] J. Mompert and R. Corbalán, Inversionless amplification in three-level systems: Dressed states quantum interference and quantum-jump analyses, *Opt. Commun.* **156**, 133 (1998).
- [21] P. Mandel, Lasing without inversion: A useful concept?, *Contemp. Phys.* **34**, 235 (1993).
- [22] M. Fleischhauer, C. H. Keitel, M. O. Scully, and C. Su, Lasing without inversion and enhancement of the index of refraction via interference of incoherent pump processes, *Opt. Commun.* **87**, 109 (1992).
- [23] Y. Zhu, Lasing without inversion in a closed three-level system, *Phys. Rev. A* **45**, R6149 (1992).
- [24] W. Tan, W. Lu, and R. G. Harrison, Lasing without inversion in a V system due to trapping of modified atomic states, *Phys. Rev. A* **46**, R3613 (1992).
- [25] G. A. Pitz, Collisional Dynamics of the Cesium D1 and D2 Transitions, (2010).
- [26] R. J. McNeal, Disorientation cross sections in optical pumping, *J. Chem. Phys.* **37**, 2726 (1962).
- [27] S. H. Autler and C. H. Townes, Stark Effect in Rapidly Varying Fields, *Phys. Rev.* **100**, 703 (1955).

- [28] M. S. Feld and A. Javan, Laser-Induced Line-Narrowing Effects in Coupled Doppler-Broadened Transitions, *Phys. Rev.* **177**, 540 (1969).
- [29] C. Wieman and T. W. Hänsch, Doppler-Free Laser Polarization Spectroscopy, *Phys. Rev. Lett.* **36**, 1170 (1976).
- [30] E. Talker, R. Zektzer, Y. Barash, N. Mazurski, and U. Levy, Atomic spectroscopy and laser frequency stabilization with scalable micrometer and sub-micrometer vapor cells, *J. Vac. Sci. Technol., B* **38**, 050601 (2020).
- [31] See the Supplemental Material at <http://link.aps.org/supplemental/10.1103/PhysRevApplied.20.014007> for a detailed calculation of the probe susceptibility in four level system and the influence of the different relaxation mechanisms on the gain signal, and the calculation of the collisional transfer rate due to presence of buffer gas.